

Quantitative Analysis of a Flat-Top Planar Waveguide Demultiplexer

Chun-Ting Lin, *Student Member, IEEE*, Yang-Tung Huang, *Member, IEEE*, and Jung-Yaw Huang

Abstract—A three-focal-point method is used for the design of a flat-top planar waveguide concave grating. With the Gaussian approximation a modified formula is proposed and is compared with the numerical model of the scalar diffraction theory by using a design example. The sources of loss caused by the flat-top design and the grating are taken into consideration. The optimal separation between the two outmost focal points is obtained and the spectral response of the demultiplexer with a ripple below 0.04 dB is achieved.

Index Terms—Concave grating, flat-top, planar waveguide, three-focal-point method, wavelength-division multiplexing.

I. INTRODUCTION

NOWADAYS, the increasing demand for optical bandwidths in the optical telecommunication network is driven by the explosive growth of Internet. Wavelength division multiplexing (WDM) systems use each wavelength as a separate channel. With the progress of the laser and the opto-electronic device, it is possible to have a high density of wavelengths in a single fiber and it is known as dense wavelength division multiplexing (DWDM). DWDM increases the transmission capacity of a fiber by increasing the wavelength channel numbers rather than increasing the data bit rate. Therefore, the performance of the optical network depends greatly on the spectral characteristics of the components it uses, such as the crosstalk, the passband width, and the insertion loss.

Planar waveguide demultiplexers/multiplexers, such as arrayed waveguide gratings (AWGs) and planar waveguide concave (etched) gratings, are of recent interest for wavelength-division-multiplexed fiber communication systems because of their low insertion loss, low crosstalk, high possibilities of mass production, and high spectral resolution. With the progress of semiconductor process, the sizes of the electronic or optical devices become smaller and smaller. Monolithic integration of the electronic and optical components may

be feasible in the future. In many cases, arrayed waveguide gratings face the problems of larger device sizes and extreme fabrication tolerances required for higher channel numbers and narrower channel spacing [1]. In contrast, the sizes of planar waveguide concave gratings can be much smaller than that of AWGs by five times in the equivalent applications [2]. However, a conventional planar waveguide demultiplexer gives a sharp spectral response and is temperature sensitive due to the temperature dependence of refractive indexes of waveguide materials, which limits the applications in the WDM system. Many techniques [3]–[12] have been proposed to overcome the problem by flattening the spectral response of the devices.

In this paper, a three-focal-point method, which was proposed for a flat-top planar waveguide demultiplexer [6], is used to obtain the flat-top spectral response. With a Gaussian approximation, the formula derived from the reference paper is modified to obtain the optimal half-separation a when the spot size of each Gaussian subimaging field is different from that for the output waveguide mode field. The grating is divided into three interleaved subgratings with different focal points and each focal point lies on the cross-sectional line of the ending facet for the output waveguide. Each subgrating forms subimage with approximately the same spot size and each subimage overlaps with each other.

To obtain a flattened spectral response, the central subimage focuses on the center of the ending facet for the output waveguide and the two outmost subimages are separated from each other with the distance of $2a$. For a symmetric spectral response, the peak amplitudes of the field for the two outmost subimages are designed to be identical. With the Gaussian field approximation, the value of the half-separation a determines the optimal ratio of the peak amplitude for the central subimage and the outmost subimage according to the modified formula. Moreover, a numerical model of the scalar diffraction theory [13] is introduced and used to verify the modified formula with a numerical example. The sources of loss and dispersion characteristics are considered in the numerical calculation.

II. MODIFIED FORMULA BASED ON GAUSSIAN APPROXIMATION

In this paper, the grating is composed of three interleaved subgratings with different focal points and each focal point lies on the cross-sectional line of the ending facet for the output waveguide as shown in Fig. 1 [6]. Each subimage formed by the corresponding subgrating overlaps with each other. With the Gaussian field approximation, the total field distribution with

Manuscript received March 27, 2008; revised June 18, 2008. Current version published April 17, 2009. This work was supported by the National Science Council of China under Contract NSC96-2221-E-009-111.

C.-T. Lin and J.-Y. Huang are with the Department of Photonics and Institute of Electro-Optical Engineering, National Chiao Tung University, Hsinchu 30010, Taiwan (e-mail: rhino.eo91g@nctu.edu.tw; jyhuang@faculty.nctu.edu.tw).

Y.-T. Huang is with the Department of Electronics Engineering and Institute of Electronics, and the Department of Biological Science and Technology, National Chiao Tung University, Hsinchu 30010, Taiwan (e-mail: huangyt@cc.nctu.edu.tw).

Color versions of one or more of the figures in this paper are available online at <http://ieeexplore.ieee.org>.

Digital Object Identifier 10.1109/JLT.2008.2004932

respect to the center of the ending facet for the output waveguide can be expressed as

$$E_{\text{image}}(f, x'') = E_1 \exp \left[-\frac{(x'' + a - D_s(f - f_0))^2}{w_{\text{image}}^2} \right] + E_2 \exp \left[-\frac{(x'' - D_s(f - f_0))^2}{w_{\text{image}}^2} \right] + E_3 \exp \left[-\frac{(x'' - a - D_s(f - f_0))^2}{w_{\text{image}}^2} \right] \quad (1)$$

where E_1 , E_2 , and E_3 denote the peak amplitudes of the three subimages, respectively, a denotes the half-separation between the two outmost subimages, D_s denotes the spatial dispersion coefficient of the grating along the x'' -axis, f denotes the frequency of the light, f_0 denotes the central frequency, and w_{image} denotes the spot size of each Gaussian subimage (the spot sizes for three subimages are approximately the same since the subgratings are interleaved [6]). To obtain a symmetric spectral response, E_1 and E_3 are designed to be identical. The effective half widths of the input and output waveguides for the fundamental modes are w_{inwg} and w_{outwg} , respectively. The spectral response of one channel can be obtained from the following overlap integral over the whole cross section of the ending facet for the output waveguide [6]

$$I(f) = \left| \int E_{\text{outwg}}(f, x'') \cdot E_{\text{image}}^*(f, x'') dx'' \right|^2 \quad (2)$$

where $E_{\text{outwg}}(f, x'')$ denotes the Gaussian mode field distribution of the output waveguide and has the form

$$E_{\text{outwg}}(f, x'') = \exp \left[-\left(\frac{x''}{w_{\text{outwg}}} \right)^2 \right]. \quad (3)$$

After the operation of convolution, the spectral response can be expressed as

$$I(f) = \left\{ 2E_1 \exp \left[-\frac{a^2 + D_s^2(f - f_0)^2}{w_{\text{image}}^2 + w_{\text{outwg}}^2} \right] \times \cosh \left[\frac{2aD_s(f - f_0)}{w_{\text{image}}^2 + w_{\text{outwg}}^2} \right] + E_2 \exp \left[-\frac{D_s^2(f - f_0)^2}{w_{\text{image}}^2 + w_{\text{outwg}}^2} \right] \right\}^2. \quad (4)$$

To obtain a flat spectral response, the curvature of the spectral response in (2) at the central frequency f_0 should be zero, and E_2/E_1 can be obtained as

$$\frac{E_2}{E_1} = 2 \exp \left(-\frac{a^2}{w_{\text{image}}^2 + w_{\text{outwg}}^2} \right) \left(\frac{2a^2}{w_{\text{image}}^2 + w_{\text{outwg}}^2} - 1 \right). \quad (5)$$

This equation shows that the ratio E_2/E_1 is a function of the half-separation a when the spot size of each subimage and the effective half width of the output mode field are determined.

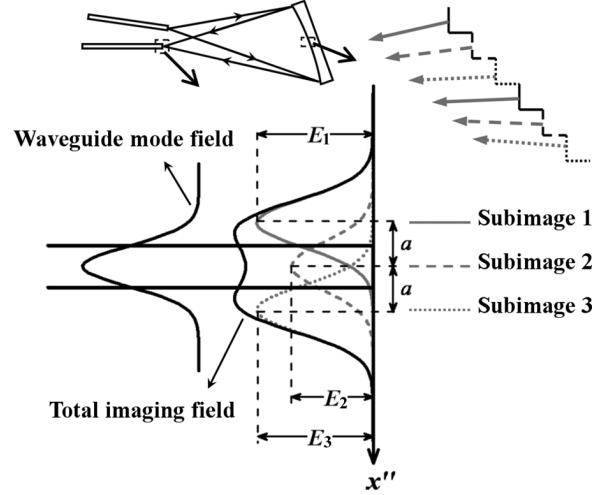


Fig. 1. Schematic figure for the three-focal-point method based on the Gaussian approximation.

III. DESIGN EXAMPLE AND NUMERICAL ANALYSIS

In this section, a planar waveguide concave grating based on the recursive definition of facet positions is introduced [13] and it was first proposed by McCreer in 1996. Simulation results show that a concave grating of the classical Rowland circle design suffers from the spherical aberration more seriously than that for the recursive-definition design [14]. The recursive-definition design is more potential and predominate than other designs. One least constraint function must be first defined. The free-aberration position of each groove is determined by the solution of the root for this constraint function, i.e., [13]

$$F(x_i, y_i) = r_{1,i} + r_{2,i} + im\lambda_0/n_{\text{eff}} - r_{1,0} - r_{2,0} = 0 \quad (6)$$

where (x_i, y_i) denotes the location of the vertex for the i th groove, $r_{j,i}$ denotes the distance between (a_j, b_j) and (x_i, y_i) as shown in Fig. 2, m denotes the diffraction order, λ_0 denotes the design wavelength, and n_{eff} denotes the effective index of the wave propagated in the slab waveguide. The tilt angle θ_i of the i th facet with respect to the x axis is determined by the following equation [13]:

$$\frac{\partial F(x_i, y_i)}{\partial x} \cos \theta_i + \frac{\partial F(x_i, y_i)}{\partial y} \sin \theta_i = 0. \quad (7)$$

Light launched from the input waveguide is diffracted by the grating, focused to the position along the imaging curve, and guided into different output waveguides according to the corresponding wavelengths. The focal equation of the concave grating has the following form [15]:

$$\frac{\cos \alpha}{R} - \frac{\cos^2 \alpha}{r_{1,0}} + \frac{\cos \beta(f)}{R} - \frac{\cos^2 \beta(f)}{r_{2,0}(f)} = 0 \quad (8)$$

where α and β denote the incident angle and the diffraction angle of the input Gaussian beam at the grating pole, respectively, R is the effective radius of the grating. The numerical model of the scalar diffraction theory for the concave grating in

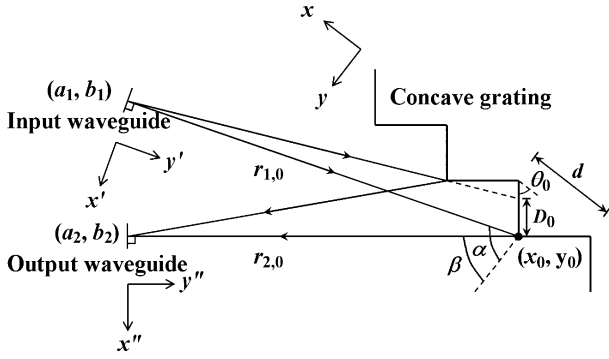


Fig. 2. Schematic figure of the light propagated in the slab waveguide and diffracted by the concave grating.

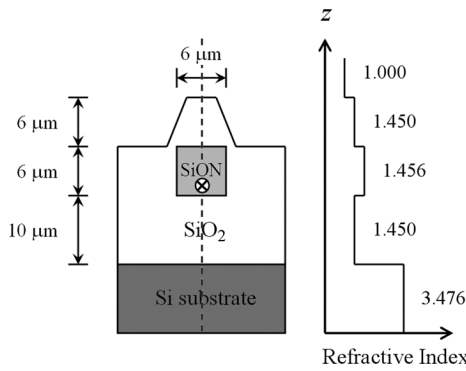


Fig. 3. Cross-sectional views of the input and output channel waveguides.

the planar waveguide was first proposed in 1995 [16], and the field formula is used in our analysis

$$E_{\text{image}}(f, x'') = E_0 \sum_i \frac{D_i n_{\text{eff}} f w_{\text{inwg}} \sqrt{\pi}}{c \sqrt{r_{1,i}} \cdot r_{2,i}} \cdot \exp[-(\gamma/\sigma)^2] \cdot \sin c[kD_i/2 \cdot (\sin \alpha' + \sin \beta')] \cdot \exp[ik(r_{1,i} + r_{2,i})], \quad (9)$$

where D_i denotes the effective facet width of the i th grating facet, w_{inwg} denotes the effective half width of the input waveguide, γ ($-\sigma \leq \gamma \leq \sigma$) denotes the angle between the ending facet normal for the input waveguide and light divergence to the i th grating facet, σ ($= \lambda_0/\pi n_{\text{eff}} w_{\text{inwg}}$) denotes the half angle for the Gaussian beam divergence at $1/e$ amplitude, k denotes the propagation constant in the slab waveguide, α' and β' denote the incident angle and the diffraction angle with respect to the i th grating facet normal, respectively.

A design example of the concave grating in silica-on-silicon is used to illustrate the three-focal-point method. The input and output channel waveguides consist of the SiON core layer with a $6 \times 6 - \mu\text{m}^2$ cross-sectional area surrounded by the SiO₂ cladding layer as shown in Fig. 3. The slab waveguide consists of a 6- μm -thick SiON core layer with the upper 6- μm -thick and lower 10- μm -thick SiO₂ cladding layers as shown in Fig. 4. The grating is achieved by etching a trench to the lower cladding layer and then coated with metal at the back wall. Therefore, light is reflected, diffracted, and focused by the metalized concave grating.

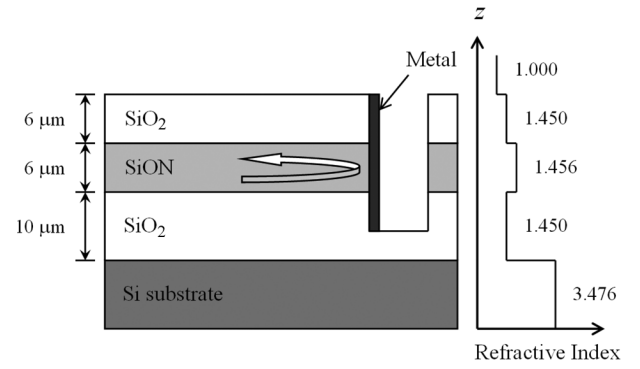


Fig. 4. Side view of the slab waveguide.

The following parameters are chosen: $n_{\text{core}} = 1.456$ for the refractive index of the core layer, $n_{\text{cladding}} = 1.450$ for the refractive index of the cladding layer, $n_{\text{si}} = 3.476$ for the refractive index of the silicon substrate at an operating wavelength of 1550.12 nm, the effective numerical aperture NA of 0.13 for the input waveguide which is the same as that for the commercial single-mode fiber, 81 channels in the C-band with the channel spacing $\Delta\lambda_{\text{channel}} = 0.4$ nm (50 GHz) from 1528.77 nm to 1560.61 nm according to ITU grids [17], $\alpha = 60^\circ$ for the incident angle at the grating pole, the diffraction order $m = 16$, $d = 10 \mu\text{m}$ for the period of the grating facet blazed at an angle obtained from (7), $N = 968$ for the total number of periods, $r_{1,0} = r_{2,0} = 35000 \mu\text{m}$ for the distances from the end of the input waveguide and the end of the design output waveguide to the grating pole, and $R = 67011 \mu\text{m}$ for the effective radius of the grating. By using the transfer-matrix method [18], the effective indexes of the TE and TM modes are obtained as 1.45393 and 1.45392, respectively. The propagation losses due to the leakages to the silicon substrate for both modes are less than 0.03 dB/cm when the thickness of the lower cladding layer is higher than 10 μm .

The E-field distribution for the TE mode within the slab waveguide in Fig. 4 is shown in Fig. 5. The effective half widths, w_{inwg} and w_{outwg} , of the input and output waveguides for the fundamental modes along the x' axis and the x'' axis are 4.91 μm obtained with BeamPROP software from R-Soft and the half angle σ for the beam divergence can be obtained as 3.96° . The spot size w_{image} of each subimage along the x'' axis is 5.85 μm ($w_{\text{image}} = 1.19w_{\text{outwg}}$). The spectral response of each channel can be obtained from the overlap integral over the whole cross section of the ending facet for the output waveguide

$$I(f) = \frac{|\int E_{\text{outwg}}(f, x'') \cdot E_{\text{image}}^*(f, x'') dx''|^2}{\int |E_{\text{outwg}}(f_0, x'')|^2 dx'' \cdot \int |E_{\text{image}}(f_0, x'')|^2 dx''} \cdot \Gamma \quad (10)$$

where Γ denotes the loss attributed to the grating or the waveguide including the undesired-order loss and the propagation loss. Here, the fiber coupling loss is not considered. The undesired-order loss, which comes from the diffraction of light into undesired adjacent orders, is one of the main sources of loss.

To make a comparison between the modified formula derived in (5) and the numerical modeling of the scalar diffraction theory for the three-focal-point method, we take the TE mode

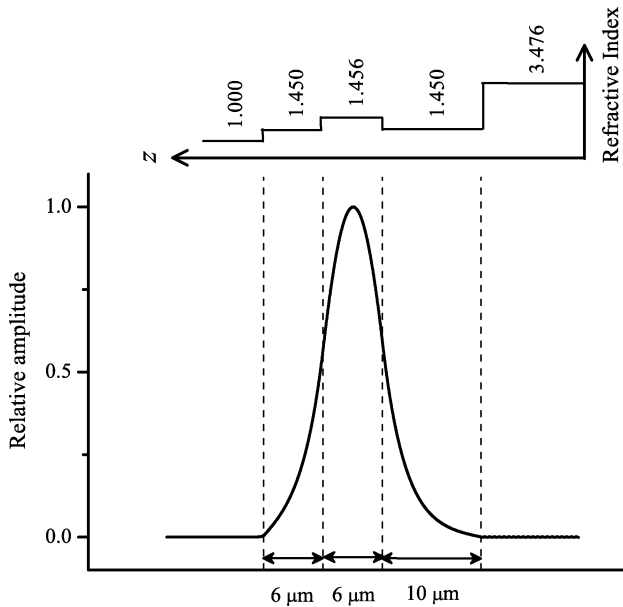


Fig. 5. E-field distribution for the TE mode within the slab waveguide as shown in Fig. 4.

for example. All computer program codes for the simulation are written in Fortran 90. If the subgratings are interleaved, the ratio of the peak amplitudes of the subimages is approximately equal to the ratio of the facet numbers of the corresponding subgratings [6]. So we can adjust the ratio of the facet numbers of subgrating 2 and subgrating 1 to adjust the ratio E_2/E_1 . If the grating pole is located at the origin of the coordinates, after determining the arrayed sequence of the facets of the subgratings the x axis coordinate position of the vertex of the i th groove can be obtained as

$$x_i = id_k = \frac{im\lambda_k}{n_{\text{eff}} \cdot (\sin \alpha + \sin \beta)} \quad (11)$$

where d_k denotes the grating period of subgrating k , m denotes the diffraction order, λ_k denotes the central wavelength of subgrating k , n_{eff} denotes the effective index in the slab waveguide, α denotes the incident angle at the grating pole, and β denotes the diffraction angle at the grating pole. The order m for each subgrating is identical but with the different grating period and central wavelength to obtain a flat-top spectral response. Then the y axis coordinate position y_i can be obtained from the solution of the root for (6). This multigrating method in which each subgrating has its own path-length increment and central wavelength has also been used in the AWG device design [4].

The optimal half-separation a can be obtained when the spectral response with a minimum ripple is achieved. The ripple is defined as the maximum difference among three extremum points within -3 -dB passband of one channel. Fig. 6 shows the ratio E_2/E_1 as a function of a for the cases of the Gaussian approximation and our numerical model where the x axis is calibrated in w_{outwg} . It shows that the deviation between the two curves becomes serious as the ratio E_2/E_1 is close to unity and the two curves have the same E_2/E_1 value of 0.7 when the optimal half-separation a is $1.52w_{\text{outwg}}$. For the case of the Gaussian approximation, only the amplitude term of the

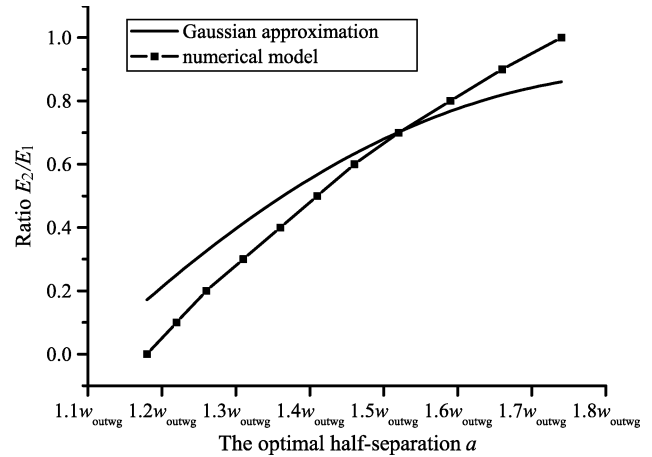


Fig. 6. E_2/E_1 versus the optimal half-separation a as $w_{\text{image}} = 1.19w_{\text{outwg}}$.

imaging field is taken into consideration as shown in (1). For the case of our numerical model, both the amplitude and phase terms of the imaging field are taken into consideration as shown in (9). So there exists the difference between the two curves for the cases of the Gaussian approximation and the numerical model as shown in Fig. 6. Without considering the scattering loss and side-wall tilt loss at the grating facet, the spectral responses of the central channel for the two cases as $E_2/E_1 = 0.7$, $a = 1.52w_{\text{outwg}}$, and $w_{\text{image}} = 1.19w_{\text{outwg}}$ are shown in Fig. 7. The spatial dispersion coefficient in our case is $D_s = 0.569 \mu\text{m}/\text{GHz}$. The insertion loss for the case of our numerical model is 4.40 dB, where 2.19 dB comes from the excess loss for the flat-top design and 2.21 dB comes from the loss Γ in (10) which is predominated by the undesired-order term. The -1 -dB passband width for the case of the Gaussian approximation is larger than that for the case of our numerical model due to no phase term of the imaging field being taken into consideration. As mentioned in Section II, for a symmetric spectral response the peak amplitudes E_1 and E_3 are designed to be identical with identical facet numbers. However, E_1 and E_3 are slightly different due to the different effective widths of adjacent facets and therefore it increases the ripple in the spectral response.

The total field distribution E_{image} of the image and the field profile E_{outwg} of the output fundamental mode at the ending facet of the output waveguide are shown in Fig. 8. To obtain a flat-top spectral response, the imaging field distribution is just like camelback. For the case of our numerical model, the -1 -dB passband width and the crosstalk versus the ratio E_2/E_1 with the channel spacing of 50 GHz for the central channel are shown in Fig. 9. It shows that the -1 -dB passband width increases as the ratio E_2/E_1 increases, while the decreased (better) crosstalk is obtained. The optimal half-separation a is obtained with a minimum ripple, and the ripple is below 0.04 dB which is shown in Fig. 10. The excess loss, the coupling loss from the slab waveguide to the output channel waveguide, versus the ratio E_2/E_1 is shown in Fig. 11. Fig. 12 shows the spectral responses of the central five channels with and without the flat-top designs for the undesired-order loss of 2.21 dB. It is shown that the flattened spectral responses can be obtained but the insertion loss will be

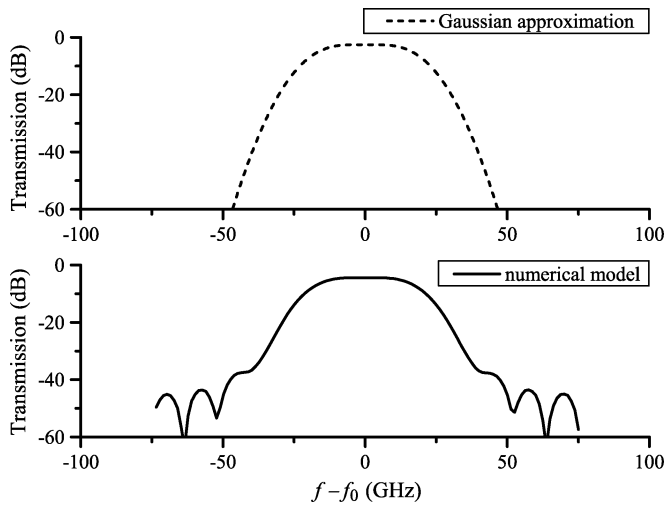


Fig. 7. Flattened spectral responses of the central channel for the two cases of the Gaussian approximation and the numerical model as $E_2/E_1 = 0.7$, $a = 1.52w_{\text{outwg}}$, and $w_{\text{image}} = 1.19w_{\text{outwg}}$.

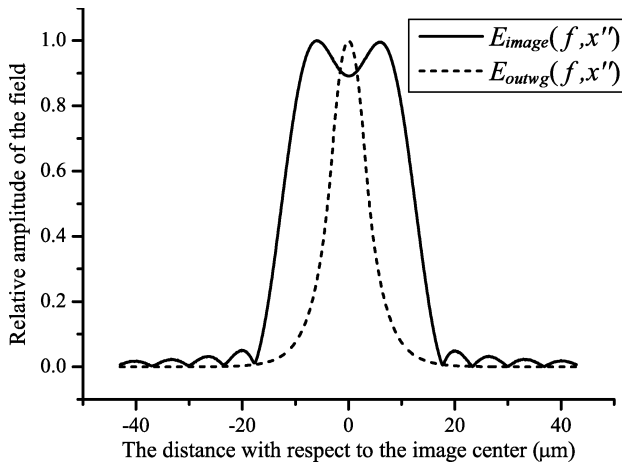


Fig. 8. Total field distribution E_{image} of the image and the field profile E_{outwg} of the output fundamental mode at the ending facet of the output waveguide.

sacrificed. The above simulation results show that the passband width for the flat-top design can be changed by changing the ratio E_2/E_1 , which then determines the optimal half-separation a as shown in Fig. 6. More numerical examples in Figs. 13 and 14 show that the value of the intersection point of the two curves decreases as the spot size of the subimage decreases and the intersection point falls on a point with a ratio E_2/E_1 of 0.5 and an optimal half-separation a of $1.24w_{\text{outwg}}$ as $w_{\text{image}} = w_{\text{outwg}}$. At the intersection point, the optimal half-separation a obtained from (5) has the same value with that obtained from the computer simulation by using our numerical model. When a changes as w_{image} changes for the assigned values of E_2/E_1 and w_{outwg} in (5), the intersection points of the two curves in Figs. 13 and 14 also change as w_{image} changes due to the different changes of E_{image} for the two cases.

The chromatic dispersion characteristic D_C is expressed as [6]

$$D_C(\lambda) = \frac{d\tau_d}{d\lambda} \quad (12)$$

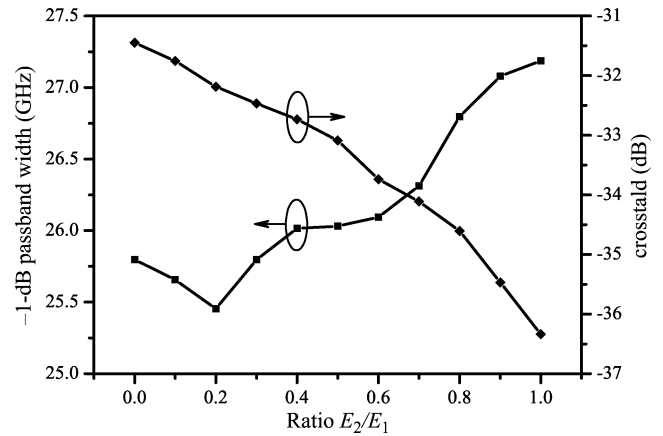


Fig. 9. -1 -dB passband width and the crosstalk versus the ratio E_2/E_1 with the channel spacing of 50 GHz for the central channel as $w_{\text{image}} = 1.19w_{\text{outwg}}$.

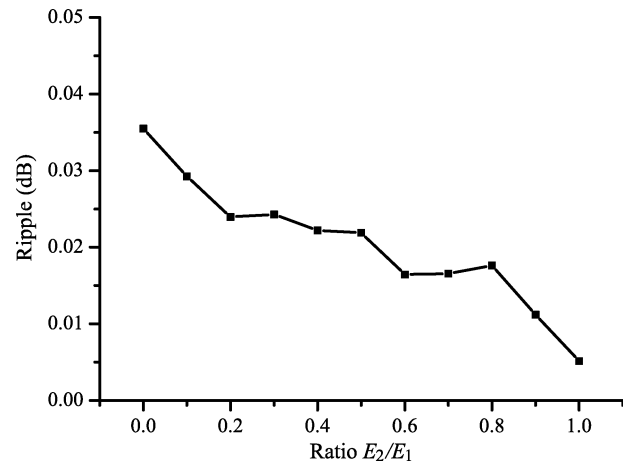


Fig. 10. Ripple versus the ratio E_2/E_1 as $w_{\text{image}} = 1.19w_{\text{outwg}}$.

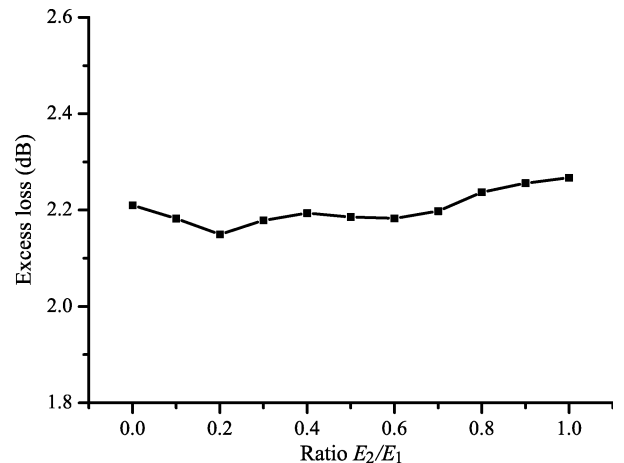


Fig. 11. Excess loss versus the ratio E_2/E_1 as $w_{\text{image}} = 1.19w_{\text{outwg}}$.

where τ_d is the group delay given by [6]

$$\tau_d \approx \frac{\lambda_0^2}{2\pi c} \frac{d\Phi(\lambda)}{d\lambda} \quad (13)$$

and where c is the velocity of the light in vacuum, and $\Phi(\lambda)$ is the phase response obtained from the overlap integral

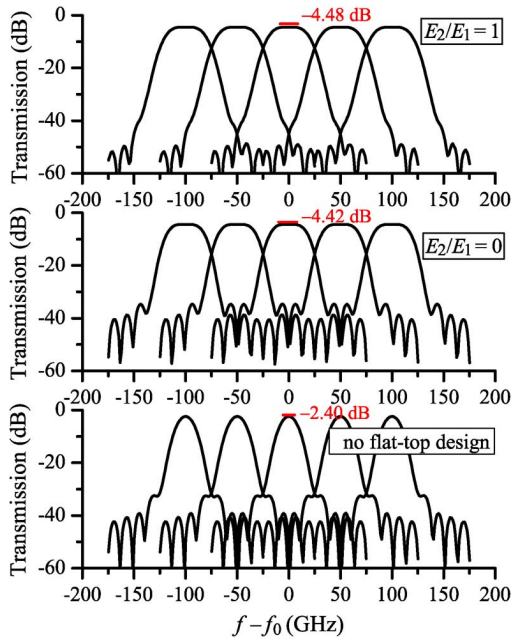


Fig. 12. Flattened spectral responses of the central five channels with and without the flat-top design for the channel spacing of 50 GHz as $w_{\text{image}} = 1.19w_{\text{outwg}}$.

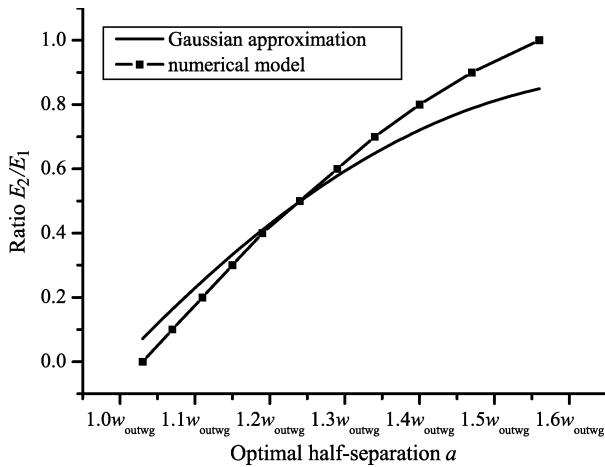


Fig. 13. E_2/E_1 versus the optimal half-separation a as $w_{\text{image}} = w_{\text{outwg}}$.

$\int E_{\text{image}}(f, x'') \cdot E_{\text{outwg}}^*(f, x'') dx''$. The chromatic dispersion characteristics are shown in Fig. 15 for the cases with and without the flat-top designs. It shows that the flat-top design has the better chromatic dispersion characteristic than that without the flat-top design. The chromatic dispersion characteristic for the case of the flat-top design ranges from -12.35 to 8.91 ps/nm within the -1 -dB passband width. The flat-top design has the flatter spectral response within the passband resulting in the slowly-changing phase response so it has the better chromatic dispersion characteristic.

IV. CONCLUSION

In this paper, a modified formula for the three-focal-point method is proposed and compared with a numerical model of the scalar diffraction theory by a design example. Simulation results show that the deviation between the two cases becomes serious

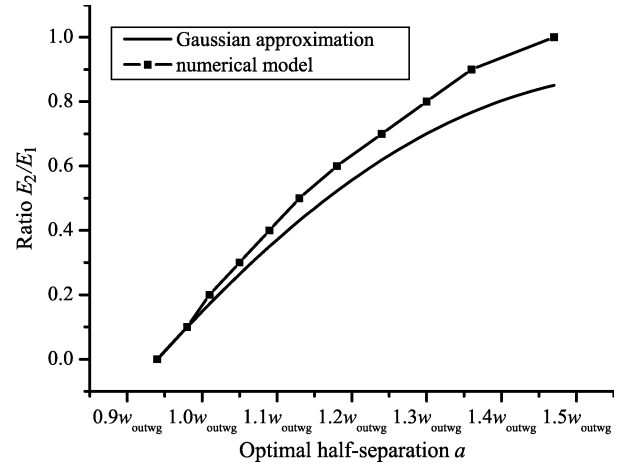


Fig. 14. E_2/E_1 versus the optimal half-separation a as $w_{\text{image}} = 0.88w_{\text{outwg}}$.

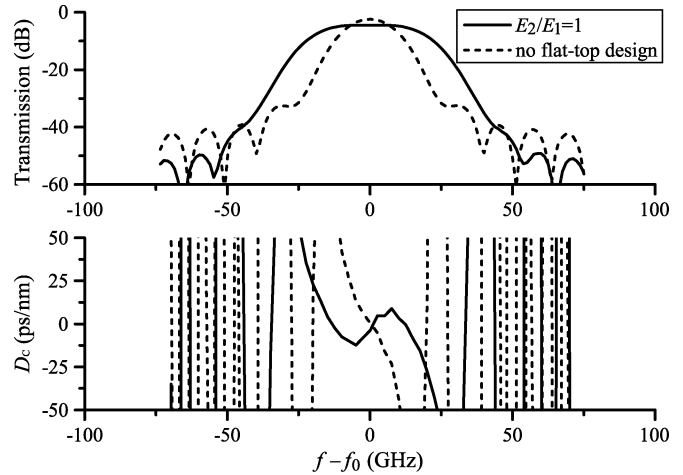


Fig. 15. Spectral responses and the chromatic dispersion characteristics with and without the flat-top design as $w_{\text{image}} = 1.19w_{\text{outwg}}$.

as the ratio E_2/E_1 approaches unity and the optimal half-separation a can be approximately obtained using the modified formula. The changed passband width can be achieved by changing the ratio E_2/E_1 . The chromatic dispersion characteristic is also considered in this paper. It is feasible to achieve the flat-top planar waveguide concave grating using the three-focal-point method.

ACKNOWLEDGMENT

The authors would like to thank H.-H. Lin at Industrial Technology Research Institute, Hsinchu, Taiwan, for the simulation discussions and the continuous encouragement.

REFERENCES

- [1] K. Takada, M. Ade, T. Shibita, and K. Okamoto, "A 25-GHz-spaced 1080-channel tandem multi/demultiplexer covering the S-, C-, and L-bands using an arrayed-waveguide grating with Gaussian passbands as primary filter," *IEEE Photon. Technol. Lett.*, vol. 14, no. 5, pp. 648–650, May 2002.
- [2] S. Janz, A. Balakrishnan, S. Charbonneau, P. Cheben, M. Cloutier, A. Delâge, K. Dossou, L. Erickson, M. Gao, P. A. Krug, B. Lamontagne, M. Packirisamy, M. Pearson, and D.-X. Xu, "Planar waveguide echelle gratings in silica-on-silicon," *IEEE Photon. Technol. Lett.*, vol. 16, no. 2, pp. 503–505, Feb. 2004.

- [3] M. R. Amersfoort, J. B. D. Soole, H. P. LeBlanc, N. C. Andreadakis, A. Rajhel, and C. Caneau, "Passband broadening of integrated arrayed waveguide filters using multimode interference couplers," *Electron. Lett.*, vol. 32, no. 5, pp. 449–451, Feb. 1996.
- [4] A. Rigny, A. Bruno, and H. Sik, "Multigrating method for flattened spectral response wavelength multi/demultiplexer," *Electron. Lett.*, vol. 33, no. 20, pp. 1701–1702, Sep. 1997.
- [5] C. Dragone, "Efficient techniques for widening the passband of a wave-length router," *J. Lightw. Technol.*, vol. 16, no. 10, pp. 1895–1906, Oct. 1998.
- [6] Z. Shi and S. He, "A three-focal-point method for the optimal design of a flat-top planar waveguide demultiplexer," *IEEE J. Sel. Top. Quantum Electron.*, vol. 8, no. 6, pp. 1179–1185, Nov./Dec. 2002.
- [7] J.-J. He, "Phase-dithered waveguide grating with flat passband and sharp transitions," *IEEE J. Sel. Top. Quantum Electron.*, vol. 8, no. 6, pp. 1186–1193, Nov./Dec. 2002.
- [8] C. R. Doerr, L. W. Stulz, and R. Pafchek, "Compact and low-loss integrated box-like passband multiplexer," *IEEE Photon. Technol. Lett.*, vol. 15, no. 7, pp. 918–920, Jul. 2003.
- [9] J. Song, D. Pang, and S. He, "A planar waveguide demultiplexer with a flat passband, sharp transitions and a low chromatic dispersion," *Opt. Commun.*, vol. 227, pp. 89–97, 2003.
- [10] Z. Shi, J.-J. He, and S. He, "An analytic method for designing passband flattened DWDM demultiplexers using spatial phase modulation," *J. Lightwave Technol.*, vol. 21, no. 10, pp. 2314–2321, Oct. 2003.
- [11] X. Chen, J. N. McMullin, C. J. Haugen, and R. G. DeCorby, "Planar concave grating demultiplexer for coarse WDM based on confocal ellipses," *Opt. Commun.*, vol. 237, pp. 71–77, 2004.
- [12] C. Dragone, "Low-loss wavelength routers for WDM optical networks and high-capacity IP routers," *J. Lightw. Technol.*, vol. 23, no. 1, pp. 66–79, Jan. 2005.
- [13] K. A. McGreer, "Theory of concave gratings based on a recursive definition of facet positions," *Appl. Opt.*, vol. 35, no. 30, pp. 5904–5910, Oct. 1996.
- [14] C.-T. Lin, Y.-T. Huang, J.-Y. Huang, and H.-H. Lin, "Integrated planar waveguide concave gratings for high density WDM systems," in *Proc. Opt. Commun. Syst. Netw.*, Banff, AB, Canada, Jul. 19–21, 2005, pp. 98–102.
- [15] M. C. Hutley, *Diffraction Gratings*. London, U.K.: Academic, 1982, p. 228.
- [16] K. A. McGreer, "Diffraction from concave gratings in planar waveguides," *IEEE Photon. Technol. Lett.*, vol. 7, no. 3, pp. 324–326, Mar. 1995.
- [17] S. V. Kartalopoulos, *Introduction to DWDM Technology*. New York: IEEE Press, 2000, p. 184.
- [18] H. Kogelnik, "Theory of optical waveguides," in *Guided-Wave Optoelectronics*, T. Tamir, Ed. Berlin, Germany: Springer-Verlag, 1990, ch. 2.



Chun-Ting Lin (S'05) was born in Taipei, Taiwan, in 1977. He received the B.S. and M.S. degrees in electrophysics from National Chiao Tung University, Hsinchu, Taiwan, in 2000 and 2002, respectively, where he is currently working toward the Ph.D. degree in electro-optical engineering.

His current research is focused on integrated optical devices for optical communication systems.



Yang-Tung Huang (M'90) was born in Taiwan, in 1955. He received the B.S. degree in electrophysics and the M.S. degree in electronics from National Chiao Tung University, Taiwan, in 1978 and 1982 respectively, and the Ph.D. degree in electrical and computer engineering (minor in optical sciences) from the University of Arizona, Tucson, in 1990.

He is a Professor at the Department of Electronics Engineering and the Institute of Electronics, and a Joint Professor at the Department of Biological Science and Technology, National Chiao Tung University, Taiwan. He has been the Director of Institute of Electronics for three years, the Director of Semiconductor Research Center for two years, and the Director of Nano Facility Center for four years. His current researches include integrated optics, photonic crystal waveguides, bio-optoelectronics, and optoelectronic switching networks.

Dr. Huang received the Outstanding Research Award from the National Science Council in 1998.



Jung-Yaw Huang received the Ph.D. from Applied Physics Department, Cornell University Ithaca, NY, in 1988.

Currently he is a Full Professor of Department of Photonics and Institute of Electro-Optical Engineering at National Chiao Tung University, Hsinchu, Taiwan. His research interests focus on the development of various optical probes for characterizing surface and bulk properties of frontier functional materials at the femtosecond and nanometer scales.